Mon. Not. R. Astron. Soc. **270,** 575–579 (1994)

Infrared spectroscopy of high-redshift quasars

A. C. Baker,[1] R. F. Carswell,[1] J. A. Bailey,[2] B. R. Espey,[3] M. G. Smith[4] and M. J. Ward[5]

[1] *Institute of Astronomy, Madingley Road, Cambridge CB3 0HA*
[2] *Anglo–Australian Observatory, PO Box 296, Epping, NSW 2121, Australia*
[3] *Department of Physics and Astronomy, University of Pittsburgh, Pittsburgh, PA 15260, USA*
[4] *Joint Astronomy Centre, 660 N. A'ohōkū Place, University Park, Hilo, HI 96720, USA*
[5] *Physics Department, Nuclear Physics Building, Keble Road, Oxford OX1 3RH*

Accepted 1994 May 3. Received 1994 April 18; in original form 1993 July 12

ABSTRACT

We present *H* and *K* spectra (showing redshifted Hα, Hβ and [O III] emission lines) of three radio-loud and three radio-quiet quasars with redshifts $z \gtrsim 2$, which were obtained using CGS4 on UKIRT. The [O III] $\lambda\lambda$4959 + 5007 lines are too weak to allow accurate determination of the redshift of the forbidden lines. The observed Balmer decrements are consistent with enhancement of Hα due to collisional excitation.

Key words: quasars: emission lines – quasars: general – infrared: galaxies.

1 INTRODUCTION

The spectra of low-redshift quasars and other active galaxies show broad-line Balmer decrements which range upwards from the case B photoionization value of $F(\mathrm{H}\alpha)/F(\mathrm{H}\beta) = 2.85$. They also generally show narrow forbidden lines from species such as [O III], in strengths that correlate with the radio flux from the object. However, at high redshifts (and higher luminosities) comparable information has only recently become available. [O III] emission has been found in high-redshift radio quasars (Kühr 1984; Carswell et al. 1991; Hill, Thompson & Elston 1993; Jackson, in preparation), and recently reported to be weak in three high-redshift radio quasars (Hill et al.).

Gaskell (1982), Wilkes (1984), Espey et al. (1989) and Corbin (1990) have shown that there are systematic redshift differences between the high-ionization and low-ionization broad lines in quasars. The example of Q1331 + 170 (Carswell et al. 1991) suggests that the low-ionization lines are at the systemic redshift, but further forbidden-line redshifts are needed to confirm this.

To address these and other points, we have started a programme of infrared observations to measure the Hα, Hβ and [O III] lines in quasars with redshifts $z \sim 2.1$–2.5. Here we consider the results from such observations of three radio-loud and three radio-quiet quasars. After outlining the observational details in Section 2, we consider the calculated line ratios and possible reddening mechanisms in Section 3, leading us to conclude in Section 4 that high Balmer decrements may be more readily explained by collisional enhancement.

2 OBSERVATIONS

We present spectra of six quasars, in the *H* and *K* windows, which were obtained using the 1–5 μm Cooled Grating Spectrometer CGS4 (Mountain et al. 1990) on the UK Infrared Telescope (UKIRT) during 1991 April and September. Some background information about the objects can be found in Table 1.

All observations were taken using the SBRC 62 × 58 InSb array, with the short camera (focal length 150 mm), using the 75 line mm^{-1} grating in first order. In this configuration, the pixels have a size of approximately 7×10^{-3} μm in the dispersion direction (approximately 3.1 arcsec per pixel spatially), so, to sample the instrument profile sufficiently, the detector was moved in the spectral direction between exposures. Some observational details are given in Table 2.

Table 1. Background information on the quasars observed. The positions and redshifts are from Hewitt & Burbidge (1987).

Object	Alternative designations	Position (1950)	Redshift z	Radio Class
*Q*0007 – 000	UM 208	0 7 42.8 – 0 4 12	2.31	Quiet
*Q*0027 + 018	UM 247 PB 5994	0 27 18.05 1 49 30.2	2.33	Quiet
*Q*0237 – 233	PKS PHL 8462 OD-263	2 37 52.72 – 23 22 8.5	2.22	Loud
*Q*1331 + 170	MC 3 PB 3977 OP 151	13 31 10.1 17 4 25	2.08	Loud
*Q*1623 + 268	KP 77	16 23 45.4 26 53 54	2.52	Quiet
*Q*1816 + 475	4C 47.48	18 16 58.70 47 35 26.9	2.23	Loud

Table 2. Observation log. All exposures taken with 75 line mm^{-1} grating, in order one, with the short (150-mm) camera.

Object	$\Delta\lambda$ (μm)	Observation Date	Exposure (mins)	$\lambda/\delta\lambda$
*Q*0007 − 000	1.41-1.80	1991 Sept 10	28	245
	1.94-2.33	1991 Sept 10	11	340
*Q*0027 + 01	1.41-1.80	1991 Sept 8	24	245
	1.94-2.33	1991 Sept 8	18	340
*Q*0237 − 233	1.41-1.78	1991 Sept 8	24	245
	1.94-2.33	1991 Sept 8	16	340
*Q*1331 + 170	1.41-1.64	1991 Apr 7	115	450
	1.95-2.34	1991 Apr 21	27	300
*Q*1623 + 268	1.51-1.90	1991 Sept 9	30	245
	2.16-2.55	1991 Sept 9	10	340
*Q*1816 + 475	1.41-1.80	1991 Sept 10	20	245
	1.94-2.33	1991 Sept 9	21	340

2.1 Data reduction

The data were reduced using the CGS4 data reduction system (pre-release version) and the FIGARO software package. Object and sky frames were observed in pairs, and then combined as object frame minus sky frame. A stack of such subtracted pairs was summed, and then we used the optimal extraction method of Horne (1986) to find the object spectrum (although the good alignment of the chip directed essentially all the object light into one row). We derived wavelength calibrations from comparison arc observations and sky features, which are accurate to better than 5×10^{-3} μm.

Observing conditions were good but non-photometric. To justify approximate spectrophotometry, we verified that the continua in the *H* and *K* windows matched (within the errors), and these internal checks suggest that the flux calibration is accurate to about 30 per cent. The spectra were flux-calibrated using contemporaneous observations of infrared standard stars from the UKIRT catalogue, and with the FIGARO routine IRFLUX. The spectra obtained are shown in Fig. 1, with the fits described in Section 3 superimposed.

3 ANALYSIS OF FLUXED SPECTRA

3.1 Calculation of line ratios

To calculate line fluxes, Gaussian fits to each line were made. Where a single Gaussian is clearly inadequate to fit the Hα line profile, we fit with two Gaussians to describe the line profile shape satisfactorily. This results in a fitted line redshift, z_f, a height h mJy and an observed velocity width v_o km s^{-1} for each component. The derived parameters from these fits, and the inferred line fluxes, are listed in Table 3.

The Balmer line fluxes generally include broad and narrow components. In the case of Q1623 + 268, a significant narrow core was detected in the Hα line, but the

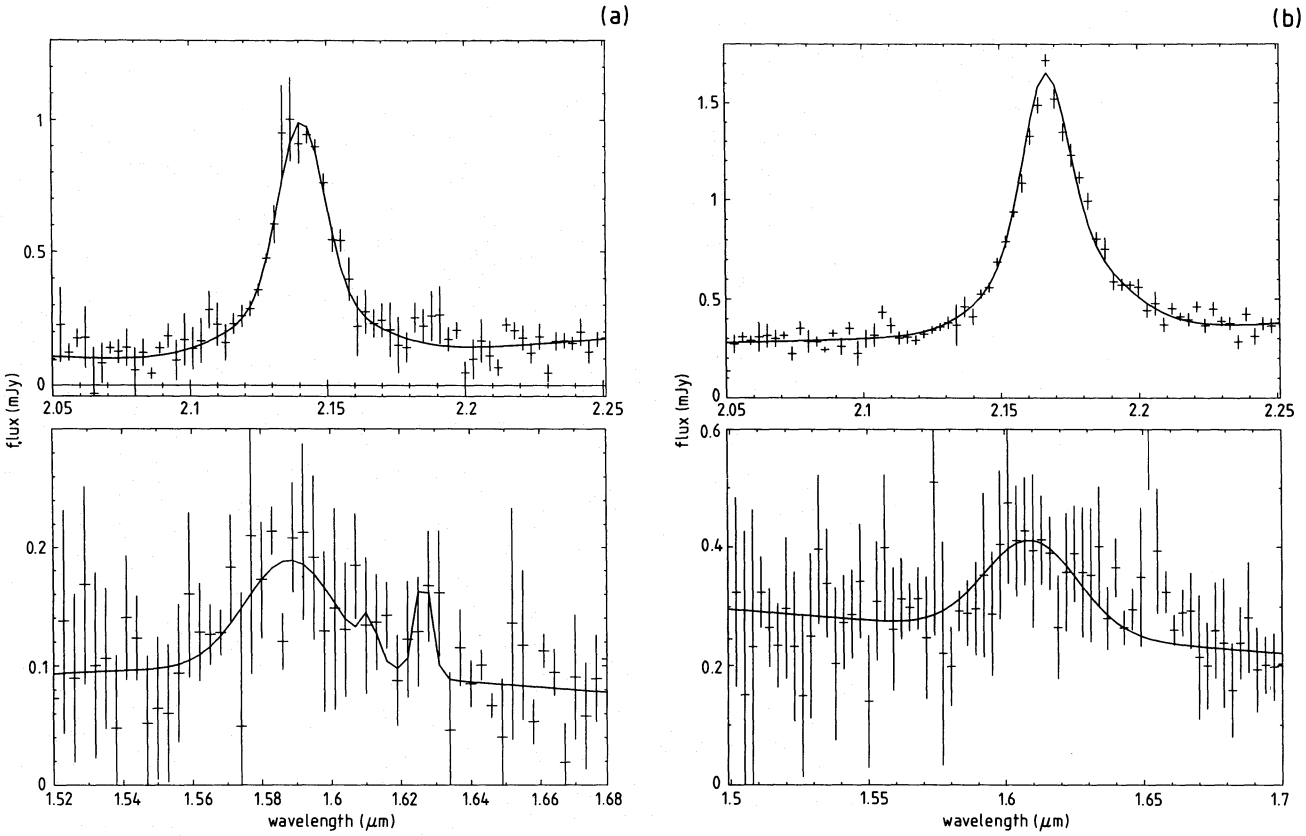

Figure 1. The flux-calibrated *H* and *K* spectra, showing (upper panels) redshifted Hα, and (lower panels) Hβ and [O III] emission lines for each object (where detected). The crosses indicate the data, showing 1σ error bars. The heavy lines indicate the adopted fits to the continua and emission lines. (a) Q0007 − 000, (b) Q0027 + 018, (c) Q0237 − 233, (d) Q1623 + 268, (e) Q1816 + 475, (f) Q1331 − 170, from Carswell et al. (1991).

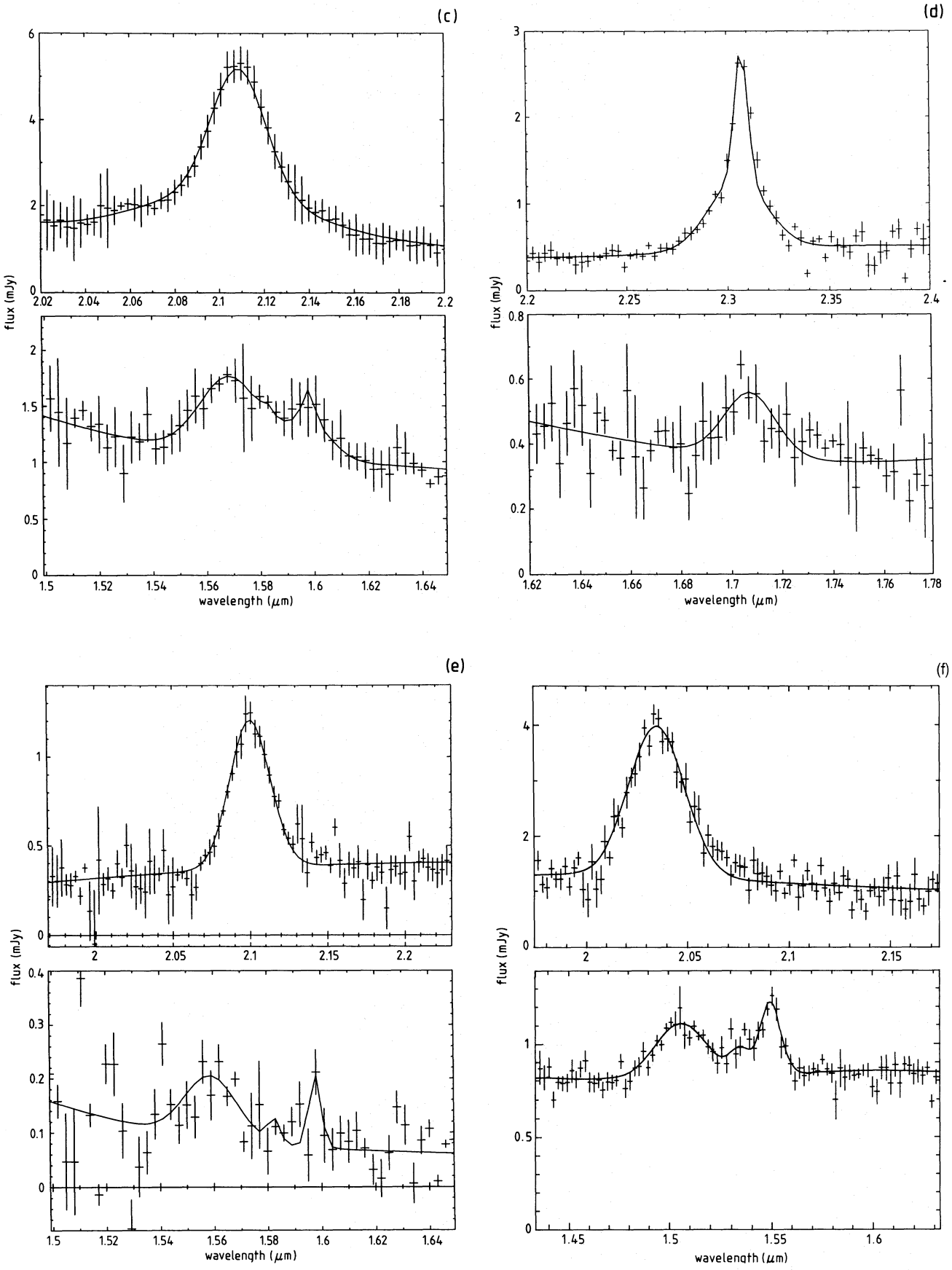

Figure 1 – *continued*

Table 3. Parameters of Gaussian line fits to Hα, Hβ and [O III] emission lines. The data for Q1331 + 170 are taken from Carswell (1991). [O III] here means blended [O III] λλ4959 + 5007. Errors are quoted as estimated 1σ error bars.[a] Limits are given at the 3σ level.[a]

Object	Lines fit	Continuum flux (mJy)	Redshift z_f	Fit Parameters Line FWHM v_0(kms^{-1})	Fit Parameters Peak height (mJy)	Observed line flux (10^{-15}ergs^{-1}cm^{-2})
Q0007 − 000	Hα	0.12	2.262	1600 ± 100	0.66 ± 0.03	
	Hα[b]		2.262	4500 ± 100	0.21 ± 0.03	32 ± 3
	Hβ	0.08	2.267	3500 ± 100	0.10 ± 0.02	7 ± 2
Q0027 + 018	Hα	0.33	2.300	2000 ± 500	0.84 ± 0.2	
	Hα		2.311	4500 ± 500	0.29 ± 0.2	49 ± 3
	Hβ	0.30	2.310	4500(fixed)[c]	0.15 ± 0.04	15 ± 4
Q0237 − 233	Hα	1.20	2.212	2500 ± 500	2.80 ± 0.5	
	Hα		2.200	7500 ± 500	1.03 ± 0.5	236 ± 68
	Hβ	1.10	2.227	3000 ± 300	0.67 ± 0.03	
	Hβ		2.287	2200 ± 300	0.33 ± 0.03	60 ± 5
	[OIII]		2.200	500(fixed)[d]	1.08 ± 0.02	3.4 ± 0.1
Q1331 + 170	Hα		2.101	4600	−[e]	65 ± 7
	Hβ		2.097	5700	−	12 ± 2
	[OIII]		2.095	1100	−	9 ± 1
Q1623 + 268	Hα[f]	0.45	2.515	600 ± 100	1.6 ± 0.1	15 ± 3
	Hα		2.512	2600 ± 100	0.8 ± 0.1	32 ± 4
	Hβ	0.37	2.512	2500 ± 500	0.19 ± 0.06	10 ± 4
Q1816 + 475	Hα	0.30	2.20	2600 ± 100	0.80 ± 0.02	34 ± 2
	Hβ	0.10	2.20	2600(fixed)	0.11 ± 0.02	7 ± 1
	[OIII]		2.19	500(fixed)	0.15 ± 0.07	0.5 ± 0.2

[a]Note that it is the internal fitting errors that are given in this table; the photometric accuracy of these measurements is estimated to be about 30 per cent.
[b]Where the line profile fits required a second Gaussian component to account for the broad wings, these are listed separately. For Q1623+268, the fluxes of each component are also quoted separately; for other objects, the total fluxes are given.
[c]Assuming that the Hα and Hβ arise in the same region, the observed width of the Hβ can be fixed from that of Hα.
[d]This prevents the fitting program from broadening [O III] to improve the fit.
[e]Parameters taken from Carswell et al. (1991).
[f]The data are unable to constrain the presence of a narrow component in the Hβ line. See Table 4 and comments in the text regarding the implications for the Balmer decrement in this case.

Table 4. Line parameters (or 3σ limits, as estimated from the fitting errors) derived from the fits in Table 3.

Object	Flux Ratios Hα/Hβ	[OIII]/Hβ	EW(Hβ) Å
Q0007−000	4.5 ± 1.0	< 0.3	130
Q0027+018	3.3 ± 0.9	< 0.5	65
Q0237−233	3.9 ± 1.2	0.19 ± 0.03	70
Q1331+170	5.5± 0.5	0.75± 0.08	36
Q1623+268	4.7 ± 1.9[a]	< 0.3	145
	3.2 ± 1.3[b]	< 0.3	145
	6.4 ± 5.2[c]	< 0.6	73
Q1816+475	5.1 ± 0.9	0.26 ± 0.1	85

[a]Balmer decrement calculated from total observed flux in both Balmer lines.
[b]Balmer decrement calculated excluding the narrow component detected for Hα (see Table 3).
[c]Balmer decrement calculated excluding narrow components from both Balmer lines. The Hβ narrow component is calculated by assuming a case B ratio with the detected narrow Hα component.

presence of a similar component in the Hβ line could not be constrained. For the other objects, no such component was identified, and the contamination from narrow-component flux is not expected to be a significant extra source of error. Fits to the *K*-band spectra which include a contribution from [N II] are excluded by higher values of the χ^2 statistic. It is therefore possible to calculate the observed Balmer decrement $F(\mathrm{H}\alpha)/F(\mathrm{H}\beta)$, and the blended flux ratio $F([\mathrm{O\,III}])/F(\mathrm{H}\beta)$ (or an upper limit for cases in which there is no positive detection of the [O III] λλ4959 + 5007 line blend). The calculated line ratios and equivalent widths are given in Table 4. The Balmer decrement for Q1623 + 268 has been calculated three times: (i) using the total Balmer flux, (ii) excluding the narrow Hα flux, and (iii) excluding the narrow Hα flux *and* the contribution to Hβ that would be expected if the narrow-component gas were under case B conditions. The steep decrement found in calculation (iii) is too uncertain to allow any useful inferences to be drawn.

The Balmer decrements are observed to lie above the case B recombination value, in the range $3.2 < \mathrm{H}\alpha/\mathrm{H}\beta < 6.4$. Whether these departures are due to dust reddening effects

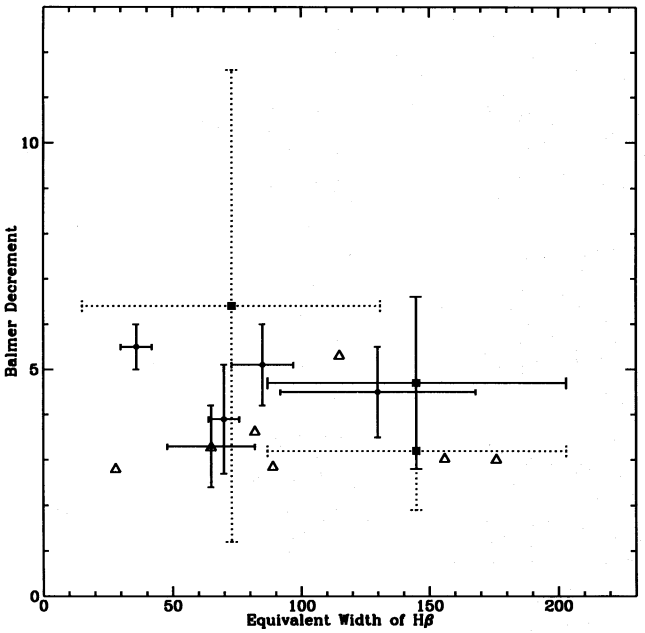

Figure 2. Scatter plot of Balmer decrement (taken from Rudy 1984) against Hβ equivalent width observed at low redshift $z<1$ (taken from Boroson & Green 1992) (open triangles), with the data from this paper superimposed (filled circles). The three alternative points for Q1623+268 are shown as filled squares; the error bars for the calculations excluding narrow components are shown dotted.

or line transfer and collisional excitation or other effects is still not determined (Grandi 1983; Osterbrock 1989).

4 DISCUSSION AND CONCLUSIONS

Only deblended estimates (radio-loud quasars) or upper limits (radio-quiet quasars) are available for the [O III]/Hβ flux. So, other than in the case of Q1331+170 (Carswell et al. 1991), no estimate of the systemic redshifts based upon those of the narrow-line gas could be determined.

We are unable to detect [O III] emission in any of our radio-quiet quasars, although the quality of the data allows only fairly weak upper limits to be determined. Hill et al. (1993) find only weak [O III] in two BAL QSOs and one other radio-quiet quasar. These results taken together raise the possibility that forbidden-line emission is generally weak in high-redshift radio-quiet quasars, although low-redshift BAL QSOs have atypically weak [O III] emission in any case (Boroson & Green 1992).

Balmer decrements Hα/Hβ in excess of 5 suggest that moderate reddening may be occurring. Dust internal to the broad-line emitting clouds would not survive (Laor & Draine 1993), where the temperature exceeds 10^4 K. The high covering fraction required of a dusty BLR is also problematic if the ionizing radiation reaches the narrow-line region. Dust in an external screen would result in a line flux ratio $F(\mathrm{Ly}\alpha)/F(\mathrm{H}\alpha)$ far higher than the observed value of ~ 2. Lyα and Balmer line profiles and redshifts generally disagree, which supports the conclusion that dust is not responsible for the observed line ratios.

Alternatively, the intrinsic emitted line ratio departs from the case B prediction. This is expected if collisional excitation of hydrogen is occurring in an optically thick region. A multizone BLR, with regions of differing density, is needed in photoionization studies to fit the observations adequately (Collin-Souffrin 1993), and is implied by observations of line velocity shifts (Espey et al. 1989; Tytler & Fan 1992).

For our high-redshift quasars, and the low-redshift quasars that appear in the samples of Boroson & Green (1992) and Rudy (1984), there seems to be no correlation between Balmer decrement and equivalent width of Hβ (see Fig. 2). Therefore objects with a larger Balmer decrement show no evidence for suppression of Hβ, which supports the suggestion that, instead, Hα is being enhanced. Collisional ionization from the $n=2$ level of hydrogen remains the most likely explanation for the higher Balmer decrements.

ACKNOWLEDGMENTS

Thanks are due to the staff at the Joint Astronomy Centre, Hilo, and to Dave Clements for constructive criticism. ACB acknowledges support from a SERC studentship award.

REFERENCES

Boroson T. A., Green R. F., 1992, ApJS, 80, 109
Carswell R. F. et al., 1991, ApJ, 381, L5
Collin-Souffrin S., 1993, in Sandqvist Aa., Ray T. P., eds, EADN Predoctoral Astrophysics School III, Central Activity in Galaxies. Springer-Verlag, Berlin, p. 97
Corbin M. R., 1990, ApJ, 357, 346
Espey B. R., Carswell R. F., Bailey J. A., Smith M. G., Ward M. J., 1989, ApJ, 342, 666
Gaskell C. M., 1982, ApJ, 263, 79
Grandi S. A., 1983, ApJ, 268, 591
Hewitt A., Burbidge G., 1987, ApJS, 63, 1
Hill G. J., Thompson K. L., Elston R., 1993, ApJ, 414, L1
Horne K., 1986, PASP, 98, 609
Kühr et al., 1984, ApJ, 284, L5
Laor A., Draine B. T., 1993, ApJ, 402, 441
Mountain C. M., Robertson D. J., Lee T. J., Wade R., 1990, in Proc. SPIE Conf. Ser., 1235, 25
Osterbrock D. E., 1989, Astrophysics of Gaseous Nebulae and Active Galactic Nuclei. University Science Books
Rudy R. J., 1984, ApJ, 284, 33
Tytler D., Fan X.-M., 1992, ApJS, 79, 1
Wilkes B. J., 1984, MNRAS, 207, 73